Optical Properties of Silicon Nanocrystals

Michel Ruben Benard

Groningen, April 2008
University of Groningen
Zernike Institute for Advanced Materials
Optical Condensed Matter Physics

This thesis is written as part of the author's Master research project at the research group Optical Condensed Matter Physics (OCMP). This research group is part of the Zernike Institute for Advanced Materials, a research institute within the Faculty of Mathematics and Natural Sciences of the University of Groningen.

The aim of research at OCMP is to identify, understand, and, if possible, control the nature of various physical phenomena and functionalities of condensed matter systems. The research is performed using a variety of linear and non-linear optical techniques and by developing microscopic models to describe the observed phenomena.

Supervisors:
Prof. dr. ir. P.H.M. van Loosdrecht
R. Augulis M.Sc.
P.J. Rizo Diago M.Sc.

Referent:
Prof. dr. ir. B.J. van Wees

Summary

Silicon nanocrystals (Si Ncs) functionalized at the surface with n-decyl chains ($C_{10}H_{21}$), have been studied using optical techniques. The absorption spectrum of the Si Ncs contains sharp peaks, in the energy range calculated with a model for strong exciton confinement in semi-conducting spheres. The fluorescence spectrum also shows a multi-peaked response, but less structured compared to the absorption spectrum. The peaked structure of the spectra can be explained by the Frank-Condon theory. Data analysis by means of this theory shows periodicy in the spectra, which can be assigned to coupled phonons. Time resolved fluorescence measurements show that the fluorescence decay is mono-exponential throughout the emission range. The decay time constant of the fluorescence is excitation wavelength and excitation intensity independent, at excitation within the absorption band. Raman scattering spectroscopy and infrared absorption spectroscopy show vibrational modes of Si Ncs. The time-resolved transient absorption shows a step-like response after the excitation. Within the time resolution no dynamics, except of coherent artifact within the time overlap of pump and probe pulses, was observed. Time-resolved transient absorption shows strong stimulated absorption in the absorption range. Outside this range no significant pump-probe response and no bleaching is observed.

Contents

Summary **3**

Contents **5**

1 Introduction **6**

2 Production of silicon nanocrystals **8**

2.1 Synthesis procedure 8

3 General theoretical background **9**

3.1 Spherical potential well 9

3.2 Frank-Condon principle 10

3.2.1 The Brownian oscillator model 12

3.3 Transient absorption 13

4 Experimental setups **14**

4.1 Continuous wave measurements 14

4.1.1 Absorption 14

4.1.2 Fluorescence spectrometer 15

4.1.3 Fluorescence OMA setup 16

4.1.4 Raman scattering spectroscopy 17

4.1.5 Infrared absorption spectroscopy 18

4.2 Time-resolved measurements 18

4.2.1 Time-resolved fluorescence 19

4.2.2 Time-resolved transient absorption spectroscopy . . . 19

5 Experimental Results **23**

5.1 Continuous Wave measurements 23

5.1.1 Absorption measurements 23

5.1.2 The Brownian oscillator model 24

5.1.3 The multi-phonon fitting model 26

5.1.4 Fluorescence measurements 29

5.1.5 Frank-Condon fluorescence fitting 31
5.1.6 Mirror image of absorption and fluorescence 32
5.1.7 Raman scattering spectroscopy 35
5.1.8 Infrared absorption spectroscopy 35
5.2 Time-resolved spectroscopy 38
5.2.1 Time-resolved fluorescence 38
5.2.2 Time-resolved transient absorption spectroscopy . . . 40

6 Discussion and Conclusions **42**

7 Acknowledgments **45**

Bibliography **47**

1 Introduction

The study of Silicon nanocrystals (Si Ncs) is an active field of research, because of their interesting physical properties, such as efficient fluorescence at room temperature, and potential applications in, for example, integrated silicon optoelectronics and fluorescent markers for biological microscopy. In addition, the Si Ncs are non-toxic and water soluble, i.e. biocompatible, which make them interesting for in vivo applications.

The Si Ncs described in this thesis are unique in the sense that the cores of the crystals are narrowly distributed in size, compared to CdTe, CdSe, and CdS Ncs produced for scientific and commercial applications [1]. These are dispersed in size by at least 5 till 10% [2]. The cores are, as shown in Fig.(1), functionalized at the surface with n-decyl chains ($C_{10}H_{21}$). The diameter of the Si Ncs is 1.57 nm [3].

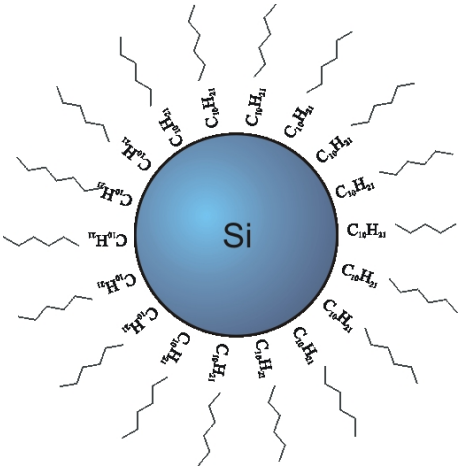

Figure 1: Schematic representation of the Si Nc with $C_{10}H_{21}$ reagents.

This funtionalization protects the Ncs from oxidation, since the highly reactive dangling bonds of the silicon crystal are partially connected to these reagents and partially to hydrogen. The aim of the project as described in this thesis is to study the dynamics of excitations in the Ncs by a variety of optical techniques.

In chapter 2 this thesis describes the synthesis of the Si Ncs. In order to understand the results of the measurements, chapter 3 aims at the general theory of the confinement of the electron-hole pair combination in the spherical potential well. To understand the electronic transitions between the ground state of the Si Ncs and higher excited state, the Frank-Condon theory is discussed in this chapter. Chapter 4 describes the experimental setups used to obtain the results to understand the dynamics of the Si Ncs. These results are discussed in chapter 5. Conclusions and discussion is given in the last part of this thesis.

2 Production of silicon nanocrystals

Since the discovery of luminescence from porous silicon [4], Si Ncs is an active field of research. Recently Si Ncs have been synthesized using a variety of techniques [5] such as laser pyrolysis [6], aerosols [7], plasma deposition [8], electrochemical etching of silicon wafers [9] and colloids [10]. The synthesis and purification of the Si Ncs used for this research are performed by Milena Rosso-Vasic and Han Zuilhof in the University of Wageningen [11], by means of the growth procedure in inverse micelles [3] as will be described in the next section.

2.1 Synthesis procedure

All steps are performed under argon during the synthesis. Tetraoctylammonium bromide (TOAB) is dispersed in dry toluene by sonication. Subsequently, $SiCl_4$ was added and dispersed by sonication. Later on, a $LiAlH_4$-solution in tetrahydrofuran (THF) was added, followed by sonication in order to form hydrogen-terminated Si Ncs in the TOAB micelles. Excess $LiAlH_4$ was oxidized with dry methanol. Alkyl-terminated Si Ncs were obtained by adding 1-dodecene and H_2PtCl_6 in methanol to the reaction mixture. The resulting Si Ncs, with $C_{10}H_{21}$ functionalization, were purified by evaporating the solvent under reduced pressure. Subsequently, the Si Ncs are dissolved in hexane. By filtrating through membrane filters the surfactant and residuals of unreacted alkene are removed.

3 General theoretical background

In this chapter the general theoretical background relevant to the experimental work on the Si Ncs will be discussed. The chapter is divided into three topics: namely, the particle in a spherical potential well approximation, for a confined electron-hole pair combination. The Frank-Condon theory is explained, to understand the electronic transitions between the ground state and the excited state. Finally the transient absorption is discussed to understand the fast dynamics of the absorption of the Si Ncs.

3.1 Spherical potential well

The most important electronic transitions for the measurements performed on Si Ncs, as described in chapter 5, are electron-hole creation and annihilation transitions. To understand the underlying physics of this process, a particle confined in a spherical potential well can be applied [12]. Developments on strong confinement in semi-conducting spheres [13] have yielded Eq.(1) for the total transition energy. This equation holds for silicon spheres smaller than the Bohr radius of bulk silicon, which is 4.9 nm [14].

$$E_t = E_g + \frac{\hbar^2 \pi^2}{2\mu R^2}, \tag{1}$$

with $\hbar$ the reduced Planck constant, μ the reduced mass of holes and electrons in silicon ($m_h^* = 0.56\ m_e$ and $m_e^* = 1.08\ m_e$) [15], and R the radius of the Si Ncs. Silicon has an indirect band gap [16] of 1.12 eV [17] and a direct band gap of 3.4 eV [18][19]. In the equation E_g represents the direct band gap of bulk silicon. The direct band gap is added to the transition energy instead of the indirect band gap, since the absorption in bulk silicon at the energy of the indirect band gap is very low compared to the absorption at the direct band gap [20] [21].

The total amount of energy calculated by employing Eq.(1) for both the confined electron and hole together with the direct optical band gap is 5.06 eV. This corresponds to a wavelength of 245 nm (40820 cm^{-1}). As

measured in chapter 5.1.1 the electronic transition to the lowest excited state is at 269 nm or 4.61 eV (37175 cm^{-1}). Therefore, it can be concluded that the theoretical calculations of the electronic transition energy compare within an error of 10 % to the measured value. Such error is not surprising since the calculations do not take the binding energy of the exciton and the Coulomb attraction into account, the radius of the Si Ncs is not known precisely, and the potential well is finite and not necessarily spherical.

3.2 Frank-Condon principle

The Frank-Condon principle gives an insight in the origin of the vibrational structure of the absorption and fluorescence spectra of the Si Ncs. At room temperature the Si Ncs are in the electronic ground state. Due to the thermal energy, several lowest vibrational states of the ground state are partially occupied. If the Si Ncs are excited by absorbing a photon, the Ncs undergo a transition to the a certain vibrational level of the electronic excited state. In principle, the behavior of the core of the Si Ncs must be taken into account during this electronic transition. The Frank-Condon principle, however, states that the electronic transition takes place much faster than the nuclei can respond due to the fact that the nuclei are much more massive than the electrons [22]. As a consequence of this, the transitions do not change the configuration ('vertical' transition) and the transitions are strongest when the overlaps between the ground and the excited state vibrational wavefunctions are the largest.

This is depicted in Fig.(2), the most occupied level of the Si Ncs in the ground state is denoted as R_e and will undergo a transition to the vibrational level of the excited state with which it has the largest vibrational wavefunction overlap. The Frank-Condon factors give the probabilities of transitions (transition dipole moments squared) from the ground state to the vibrational levels of the excited state. The Frank-Condon factor from the ground state to the n^{th} vibrational level is given by

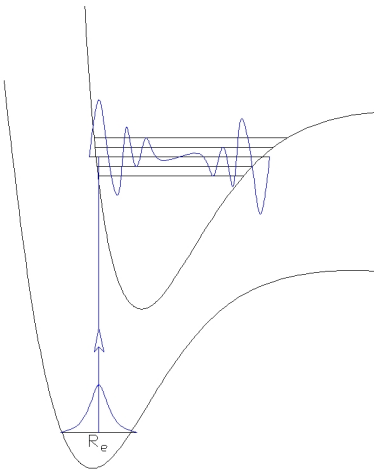

Figure 2: This figure schematically shows the wave function overlap of the ground state and a vibrational level of the excited state. The most occupied level of the Si Ncs in the ground state is denoted as R_e.

$$\frac{S^n e^{-S}}{n!}, \tag{2}$$

in which S is the probability that the transition occurs from the lowest vibrational level of the ground state to the n^{th} vibrational level of the excited state. The full spectrum including transitions from the ground state to all vibrational levels, is given by

$$\sum_{n=0}^{\infty} \frac{S^n e^{-S}}{n!} \delta(\omega - \omega_0 - n\Omega), \tag{3}$$

in which ω_0 is the energy of the electronic transition, Ω is the energy of a single phonon, and ω is the excitation energy. To dress the transition distribution with a line width, spectrum is convolved with a Gaussian:

$$I_{(\omega)} = \sum_{n=0}^{\infty} \frac{S^n e^{-S}}{n!} A e^{\frac{-(\omega-\omega_0-n\Omega)^2}{2\sigma^2}}, \tag{4}$$

in which A determines the intensity of the transition, and $2\sigma^2$ determines the width of the Gaussian, which is the broadening in the potential landscape of the transition.

3.2.1 The Brownian oscillator model

Calculations on the absorption spectrum of the Si Ncs by means of the Brownian oscillator model [23] will be explained. The zero-phonon line of the absorption spectrum is the transition from the ground state to the lowest vibrational level of the excited state, no phonons are involved. This line is set at zero, the vibrational energies are on top of the zero-phonon energy. The absorption spectrum as function of energy can be calculated by considering the real part of the Fourier transform of the damped oscillator,

$$Abs = Re \int_0^\infty e^{-g(t)} e^{i\omega t} dt, \tag{5}$$

with ω representing the harmonic oscillator frequency in time t and $g(t)$ representing the damped oscillator. For the low temperature limit $\hbar\omega >> k_bT$, the following equation for the damped oscillator holds

$$g_{(t)} = i\frac{\Delta^2}{\Omega^2} sin(\Omega t) + \frac{\Delta^2}{\Omega^2}(1 - cos(\Delta t)), \tag{6}$$

or

$$g_{(t)} = \frac{\Delta^2}{\Omega^2} - \frac{\Delta^2}{\Omega^2} e^{-i\Omega t}, \tag{7}$$

with k_b the Boltzmann constant and Δ as the intensity of the absorption peaks, which is linked to the fluorescence decay time constant. Substituting Eq.(7) in to Eq.(5) gives

$$Abs = Re \int_0^\infty e^{\frac{\Delta^2}{\Omega^2}} e^{\frac{\Delta^2}{\Omega^2} e^{-i\Omega t}} e^{i\omega t} dt. \tag{8}$$

Rewriting the absorption equation by the Taylor expansion of $e^{\frac{\Delta^2}{\Omega^2} e^{-i\Omega t}}$ yields

$$Abs = Re \int_0^\infty e^{\frac{\Delta^2}{\Omega^2}} \sum_{n=0}^{\infty} \left(\frac{\Delta^2}{\Omega^2}\right)^n \frac{1}{n!} e^{-in\Omega t} e^{i\omega t} dt, \tag{9}$$

for n vibrational levels. Eq.(9) can be rewritten as

$$Abs = \sum_{n=0}^{\infty} \left(\frac{\Delta^2}{\Omega^2}\right)^n \frac{1}{n!} e^{\frac{\Delta^2}{\Omega^2}} Re \int_0^\infty e^{i(\omega - n\Omega)t} dt, \tag{10}$$

which finally yields

$$Abs = \sum_{n=0}^{\infty} \frac{S^n e^{-S}}{n!} \delta(\omega - n\Omega). \tag{11}$$

This result convolved with a Gaussian is used in the Brownian oscillator fitting model.

3.3 Transient absorption

To study the fast dynamics of the absorption of the Si Ncs, pump-probe measurements are performed, the results of which are described in section 5.2.2. The Si Ncs are excited by the pump beam and probed by the probe beam of the setup as described in section 4.2.2. By the excitation pulse, the electrons from the ground state undergo transitions to the first excited state. Thus, the ground state is depopulated, so the absorption due to the electronic transitions from the ground state to the first excited state is reduced, so called 'bleached'. In addition, the transitions form the excited state to the ground state become possible, which is observed as stimulated emission. Finally, the transitions from the first excited state to the higher excited states are possible, since the first excited state is partly populated. In this case induced absorption is observed.

The pump-probe technique measures the transient absorption (ΔOD) of the sample of Si Ncs. A positive ΔOD, as measured in the pump-probe measurements on Si Ncs, demonstrates no bleaching and stimulated absorption.

4 Experimental setups

This section describes the experimental setups used to obtain the results as are described in section 5. This chapter is divided into two main parts, namely the continuous wave measurements and the time-resolved measurements.

4.1 Continuous wave measurements

The continuous wave (CW) measurements are performed in order to get time integrated spectra. UV and infrared (IR) absorption, fluorescence, and Raman scattering CW measurements are performed. The experimental setups will be discussed in the following sections.

4.1.1 Absorption

The absorption spectra are recorded using a Lambda 900 spectrometer from Perkin Elmer which features a double-beam optical system. One of the beams is transmitted through the sample, the other one is used as reference. The reference beam can also be transmitted through a cell with, for example, the solvent used for the sample, thus, eliminating the artifacts caused by reflections from the cell and solvent absorption. Since the reference beam is used, the spectral sensitivity of the spectrometer is the same in all the measurement range.
Fig.(3) shows the schematic representation of the absorption spectrometer. The sample in a cryostat is irradiated by a monochromatic beam, created in the monochromator. The intensity ratio of the transmitted beam through the sample and the reference is used to determine the optical density of the sample. For low temperature measurements air is the reference. The resolutions of the absorption spectrometer can be up to 0.05 nm for both the recording step size and the detection slit. The detection slit determines the resolution of the spectral range measured. The detection range for this spectrometer is from the near-IR to far UV (3300 nm to 185 nm).

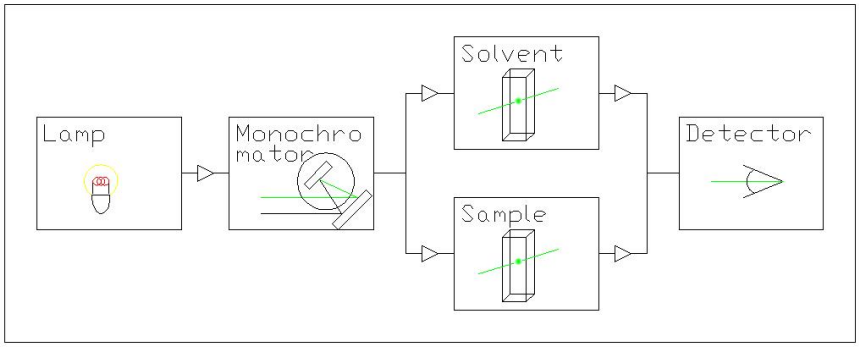

Figure 3: This figure represents the absorption spectrometer. The sample and the reference cells are irradiated by monochromatic beams, created in the monochromator. The intensity ratio of the transmitted beams is used to determine the optical density of the sample. For low temperature measurements the sample is inside a cryostat in the spectrometer.

4.1.2 Fluorescence spectrometer

The fluorescence spectrum is obtained using a Fluorlog spectrometer (Horiba Jobin Yvon). The schematic of the spectrometer is represented in Fig.(4).

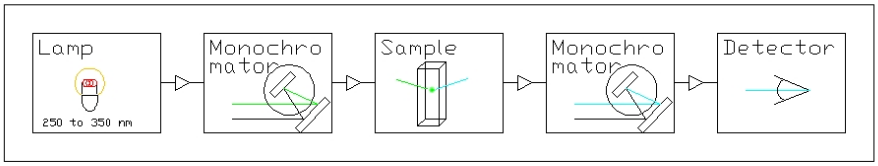

Figure 4: Schematic representation of the fluorescence spectrometer. Monochromatic light excites the sample and the fluorescence is detected integrated over time.

The fluorescence of the Si Ncs is detected by the fluorescence spectrometer. The spectral resolution of this spectrometer can be set to as high as 0.05 nm for the excitation and detection slits. For the measurements performed

on the Si Ncs a 1 nm excitation and detection bandpass was used (which is 110 cm^{-1} at 300 nm) in order to obtain a significant signal, with a good signal to noise ratio. The resolution is several nm. The spectra obtained are not corrected for the spectral response of the detectors and optics of the spectrometer since the correction curve in UV is not known. This means that the peak intensities are arbitrary. Fluorescence measurements performed with this methods are only used to obtain the excitation dependent emission spectrum of the Si Ncs.

4.1.3 Fluorescence OMA setup

To improve the resolution of the fluorescence measurements from several nanometers to 0.6 nm (58 cm^{-1} at an excitation wavelength of 260 nm), the fluorescence is recorded using the setup as represented in Fig.(5).

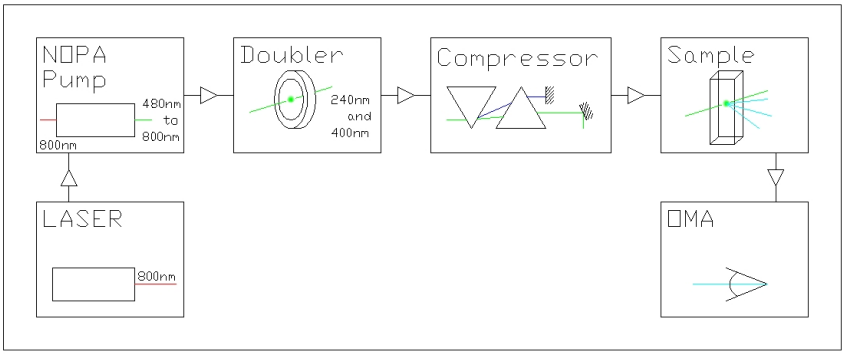

Figure 5: Schematic representation of the setup used to measure the fluorescence of the Si Ncs with an optical multi-channel analyzer.

This schematic shows the setup based on the amplified Titanium-Sapphire laser (Hurricane, Spectra Physics). The laser produces 800 nm 120 fs pulses at 1 kHz repetition rate with 700 μJ energy per pulse. A portion of the beam, with an energy per pulse of 250 μJ, is converted by the non-collinear optical parametric amplifier (NOPA)(TOPAS-White, Light Conversion Ltd.) to wavelengths between 480 and 800 nm with a pulse duration of approximately

50 fs. The output beam from the NOPA is frequency-doubled in a Beta Barium Borate (BBO) crystal of 0.2 mm, so the spectral range becomes 240 to 400 nm. The collimated and spatially filtered UV beam is focused into the sample.

The Si Ncs are excited by 250 to 270 nm pulses, at an energy of 20 nJ per pulse. This is equivalent to 20 μW integrated power. The fluorescence is detected by a CW Optical Multi-channel Analyzer (OMA) with a resolution of approximately 0.6 nm (58 cm^{-1} at 260 nm). The second diffraction order of the monochromator grating is used to double the spectral resolution and improve the throughput of the system in UV. The diode-array detector of OMA is cooled to approximately -25^{o}C for noise reduction.

4.1.4 Raman scattering spectroscopy

The Raman scattering measurements are performed [24] using a triple grating micro-Raman spectrometer (Jobin Yvon, T64000), equipped with a liquid nitrogen cooled charge coupled device detector (resolution of 2 cm^{-1} for the considered frequency interval). The experiments were performed with a 532 nm Nd:YVO4 laser. The power density on the sample was kept below 500 W/cm^2 to avoid sample degradation and to minimize heating effects.

Raman scattering occurs when light from the laser excites an electron of the Si Ncs to a virtual excited state. The electron relaxes back to a vibrational level of the ground state. The detected difference of the energy of the incident photon and the scattered photon indicates the energy difference between the initial and final vibrational levels. The transition from the lower level to a virtual excited state and back to the higher vibrational level is called the Stokes Raman scattering. The transition from the higher vibrational level to a virtual state and back to the lower level is called the anti-Stokes Raman scattering. Therefore, Raman spectroscopy provides information about the vibrational structure of the ground electronic state.

4.1.5 Infrared absorption spectroscopy

Fourier-transform infrared (FT-IR) spectroscopy is performed using the Michelson interferometer [25]. The light from the source is focused by the lens L1 and split by the beam splitter. The reflected beam reaches the detector D after it was reflected by mirror M1. The transmitted beam reaches the detector after it was reflected by mirror M2. Mirror M2 is mobile and can translate a distance Δx, the interference of the beams causes intensity oscillations at the detector. This detected interferogram is used by the spectrometer to obtain the spectral components of the light by Fourier transformation, without any spectral dispersion. A sample is positioned between lens L2 and the detectors. This sample influences the interferogram, and provides therefore information on the IR absorption in the sample. The general rule for an atom to absorb the emitted light from the spectrometer by a molecular vibration is that the electric dipole moment of the molecule must change when the atoms are displaced relatively to each other. These vibrations are called infrared active. If a vibration does not change the electrical dipole moment of the molecule, it is infrared inactive and can not be detected by means of IR absorption spectroscopy. Performing FT-IR measurements, infrared active vibrational modes of the ground electronic state are measured.
The IR measurements are performed by means of the Bruker IFS 66v/s spectrometer. The measurements are performed in vacuum, within a spectral range of 550 cm^{-1} to 4000 cm^{-1}.

4.2 Time-resolved measurements

Time-resolved spectroscopy contains, in contrast to the CW measurements as described in section 4.1, time information of the measured phenomena. In the following sections the time-resolved fluorescence and the the pump-probe setups will be discussed.

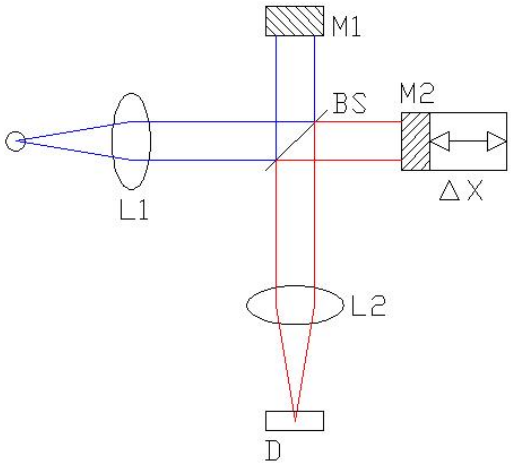

Figure 6: Schematic representation of the Michelson interferometer used in the Fourier-transform infrared spectrometer.

4.2.1 Time-resolved fluorescence

The time-resolved fluorescence measurements are performed using a streak camera and a Titanium (Ti) Sapphire (Al_2O_3) laser system. As shown in Fig.(7), the 532 nm continuous wave Verdi 5 Watt laser pumps the 76 MHz Ti:Sapphire pulsed MIRA 900-f laser, which is tunable in a spectral range of 700 to 1000 nm. The pulse picker selects and transmits the MIRA pulses with a repetition rate of 1.9 MHz. The signal is frequency-tripled by the crystals of the third harmonic generator and focused into the sample. The fluorescence of the Si Ncs is dispersed in a polychromator and detected by a C5680 Hamamatsu streak camera. For these measurements a M5677 single sweep unit detector is used. The time-range of the streak camera is set to 20 ns, which allows 200 ps resolution.

4.2.2 Time-resolved transient absorption spectroscopy

The basics of the setup used to measure the fluorescence by exciting by a pulsed lases, as described in section 4.1.2, is also used for the pump-

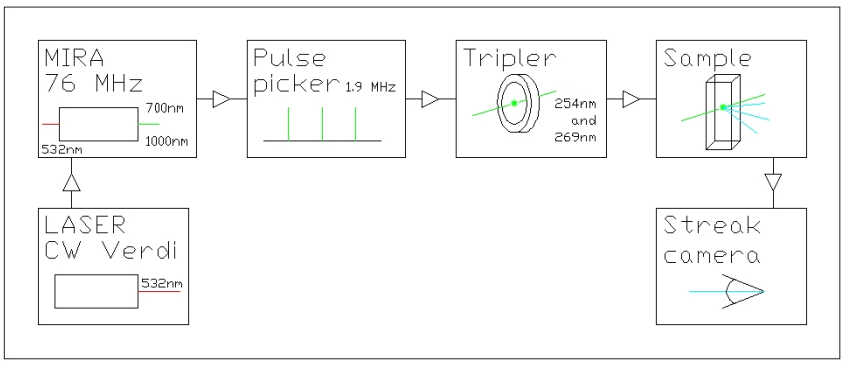

Figure 7: This schematic represents schematically the setup used to measure the time-resolved fluorescence of the Si Ncs. As can be observed, the pulsed beam is tripled and projected on the sample which will fluoresce in the UV. This fluorescence is measured by making use of a streak camera.

probe measurements. In addition, the pump-probe setup features probe and reference beams. The pump beam has an intensity of approximately 10 nJ per pulse at 250 nm, with 1.5 nm spectral width. The setup is schematically represented in Fig.(8) and is divided into two sections, as also depicted in this figure. Namely, the light generation section and the detection section.

In the light generation section the schematic shows the Titanium-Sapphire laser system (Hurricane, Spectra Physics) which emits 800 nm 120 fs 700 μJ light pulses at a repetition rate of 1 kHz. Two portions of the beam beam (250 μJ each) are converted by two NOPA's to independently spectrally tunable beams with wavelengths between 480 and 800 nm and pulse duration of approximately 50 fs. The outputs of the NOPA's is frequency doubled in a crystal of Beta Barium Borate (BBO) of 0.2 mm to 240 to 400 nm. Since the spectral width of the pulses becomes narrower (1 - 2 nm) after doubling, the pulse is stretched up to 100 - 150 fs. This limits the time resolution of the whole system to approximately 200 fs. The parts of the beams which are not frequency-doubled are separated by the compressors. The excitation wavelength of the Si Ncs is 250 nm.

At the detection section, a part of the probe beam is split by a beam

splitter and used as a reference beam. The incoming pump beam and the rest of the probe beam are focused and spatially overlapped in the sample. After the sample the pump beam is blocked. The reference beam is transmitted through the sample as well. The pump beam is chopped at 500Hz, so the sample is probed with pump and without pump. The intensities of the probe beam with pump and without pump are compared and the induced changes in transmission are calculated. The reference beam is used to eliminate the artifacts caused by intensity fluctuations in the probe beam. The probe beam can be delayed with respect to the pump beam by means of a delay line, so the time dynamics of absorption could be recorded.

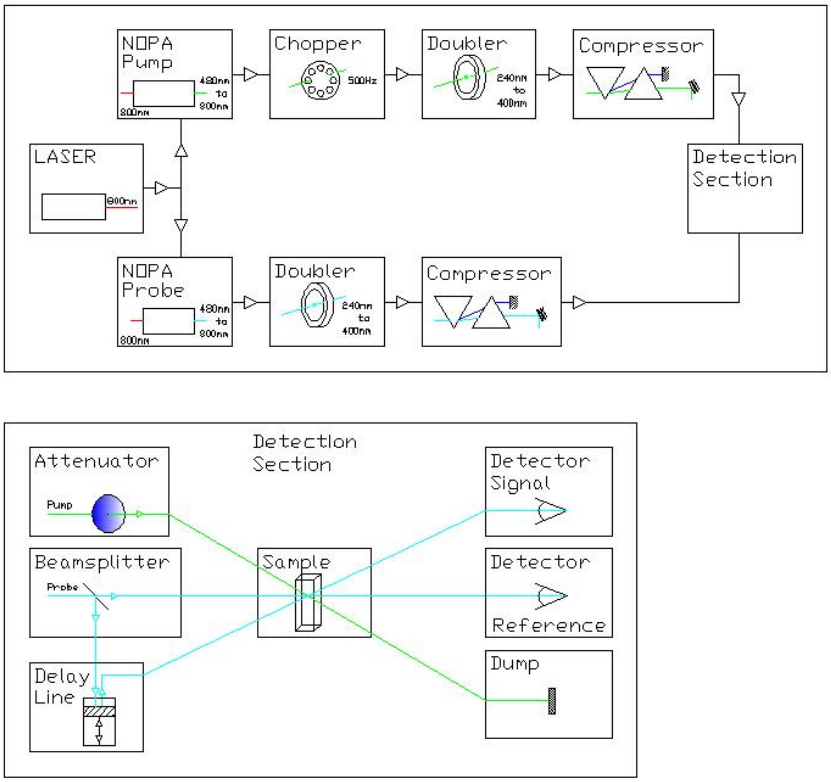

Figure 8: Schematic representation of the pump-probe setup used to determine the spectral dynamics and the difference in optical density of the sample. Two portions of the 800 nm laser beam are converted by the NOPA's to the beams in the spectral range of 480 to 800 nm. The chirps of the pulses are compensated by the compressors after the beams are frequency-doubled. The undoubled parts of the beams are separated by the compressors.

5 Experimental Results

In this chapter, the results obtained from fittings by means of the Frank-Condon and the Brownian oscillator model, as described in chapter 3, and the results obtained by employing the setups described in the previous chapter, will be discussed.

5.1 Continuous Wave measurements

The measurements are performed in order to study the structure and the optical properties of Si Ncs. Unless specified differently, the measurements are performed at room temperature with the Si Ncs placed into a 1 mm path length far-UV quartz cuvette (Q21, Starna). The concentration of Si Ncs in the solution is $2.9{\cdot}10^{-4}$ M. This section will discuss the CW measurements performed which experimental setups described in section 4.1.1 to 4.1.4. CW UV and IR absorption, fluorescence, and Raman scattering measurements are performed and the experimental results will be discussed, together with the absorption and fluorescence fittings.

5.1.1 Absorption measurements

For performing any optical measurements on Si Ncs it is necessary to know in what wavelength region the absorption of this material takes place. Therefore, the absorption of the Si Ncs is measured, as can be seen in Fig.(9).

The absorption was measured in a spectral range of 37040 cm^{-1} to 42550 cm^{-1} (235 - 270 nm). As can be observed in this figure, the absorption spectrum contains several sharp peaks. The most probable interpretation is that this structure originates from the transitions of the ground state to the the vibrational levels of the excited state (see chapter 3). Therefore, this absorption measurement probes the structure of the lowest electronic excited state. The sharp peak at 269 nm is the zero-phonon line, the transition from the ground state to the lowest vibrational level of the electronic excited state. The peak positions of the absorption spectrum has a periodicy of

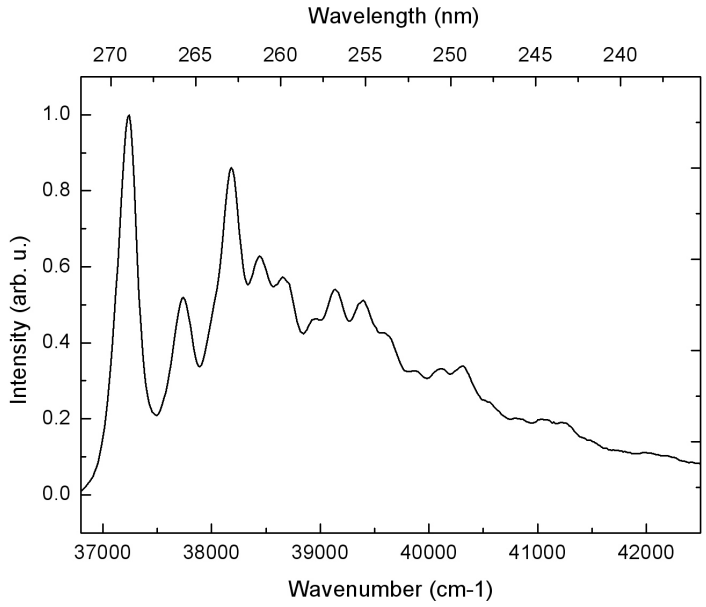

Figure 9: The absorption spectrum of Si Ncs, in wavenumbers (bottom) and wavelength (top), measured at 180 K.

957 cm^{-1}, dressed with multiple 247 cm^{-1} modes, starting from the zero-phonon line. The step size of the measurements shown in Fig.(9) and the monochromator resolution was set to 0.25 nm. As described in chapter 4, the best resolution of the absorption spectrometer is 0.05 nm. Measurements performed with this resolution resolve no additional spectral details, but the noise is increasing. Therefore a 0.25 nm resolution is chosen as optimal.

5.1.2 The Brownian oscillator model

The Brownian oscillator model discussed in chapter 3 has been fitted to the measured absorption spectrum. In order to obtain a reasonable fit, six oscillators were required, each with their own intensity Δ and frequency Ω. The result of this fitting is shown in Fig.(10), where the zero-phonon line has been shifted to zero.

As can be observed from the fitting, this model is in good correspondence to the measured absorption spectrum for low wavenumbers. By adding more

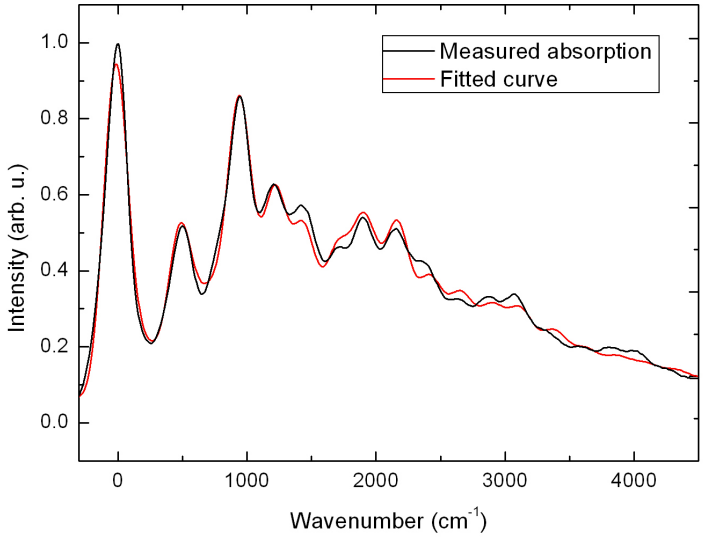

Figure 10: The absorption spectra of Si Ncs (black curve) and the fitted spectrum (red curve) obtained by means of fitting with Brownian oscillators with random frequencies.

Frequency Ω (cm^{-1})	Amplitude Δ (arb. u.)
2087	0.05194
1249	0.08833
951	0.13152
717	0.02627
503	0.04492
246	0.00515

Table 1: Fitting parameters of the Brownian fitting model.

phonons into the system, also higher wavenumbers can be fitted in better correspondence to the measured values. The fit could also be improved by coupling the phonons, which gives a higher oscillator strength at higher wavenumbers and less phonons.

The frequency of the vibrational modes obtained from this fitting is shown in table 1. The phonon frequencies from 246 and 503 cm^{-1} are expected energies for vibrations in silicon. The 717 to 2087 cm^{-1} phonons can possibly be a interpreted as e.g. coupled phonons, surface vibrations, Si-C bonds. Possibly, the discrepancy of the fit originates from the fact that the Brownian oscillator model holds for low temperatures or that phonon frequencies should be coupled.

5.1.3 The multi-phonon fitting model

It can be observed that the absorption spectrum contains a structure periodicity of 957 cm^{-1}, starting from the first clear peak which is the zero-phonon line. The peak separation energy is 247 cm^{-1}. The structure periodicity and the peak separation energies can be interpreted as a combination of interacting phonons. So the combination of one to five phonons with a frequency of 957 cm^{-1} with zero to five phonons with a frequency of 247 cm^{-1}. These frequencies are in the Brownian oscillator fitting model present as well. The curves of the two phonon fittings is shown in Fig.(11). This figure shows the 957 cm^{-1} phonons, Fig.(11(a)), the 247 cm^{-1} phonons, Fig.(11(b)), and the combination of multiple 957 cm^{-1} phonons, dressed with one to three times the 247 cm^{-1} phonons, Fig.(11(c)) to Fig.(11(e)).
The fitting parameters of this fit are the amplitude and width of the absorption peaks and two phonon frequencies. The peak positions are set by linear combinations of the phonons. The fitting parameters are shown in table 2.

This fit approaches the measured absorption very well, but it can not be concluded that the multi-phonon fitting is physically better than the Brownian oscillator. The reason for this is that the expected cross-section of transitions which involve up to ten phonons is relatively low.

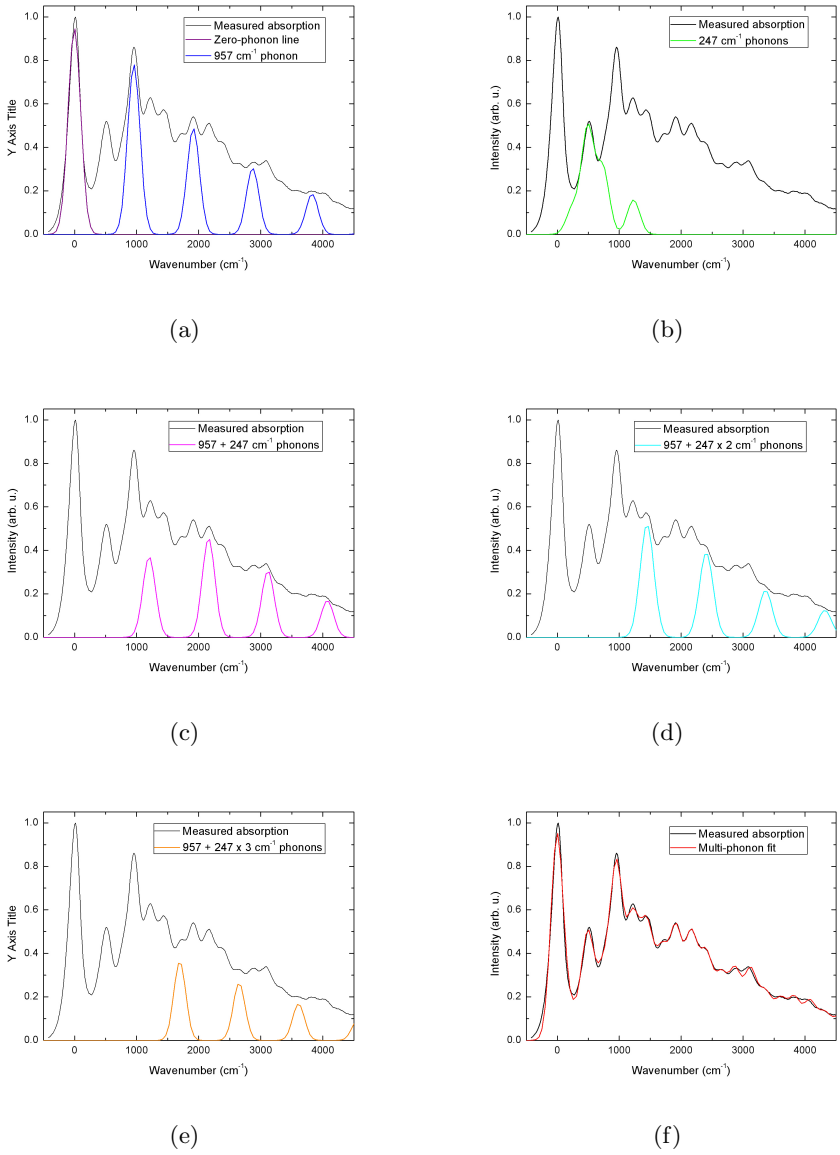

Figure 11: (a) shows the absorption spectra of Si Ncs (black curve) and the 957 cm^{-1} phonons (blue curve). (b) shows the 247 cm^{-1} phonons (green curve). (c) shows the multiple 957 cm^{-1} phonons dressed with the 247 cm^{-1} phonons (magenta curve). (d) shows the multiple 957 cm^{-1} phonons dressed with two 247 cm^{-1} phonons (cyan curve). (e) shows the multiple 957 cm^{-1} phonons dressed with three 247 cm^{-1} phonons (orange curve). (f) shows the the addition of the multi-phonon progressions (red curve).

n	m	Wavenumber (cm^{-1}) $n \cdot 957 + m \cdot 247$	Linewidth ω_0 (cm^{-1})	Amplitude (arb. u.)
0	0	0	143	0.95
1	0	957	142	0.78
2	0	1914	142	0.49
3	0	2871	142	0.31
4	0	3828	142	0.18
0	0	247	143	0.12
0	1	494	143	0.49
0	2	741	143	0.30
0	3	988	143	0.00
0	4	1235	143	0.16
1	1	1194	145	0.37
2	1	2141	145	0.46
3	1	3088	145	0.31
4	1	4035	145	0.17
1	2	1451	158	0.52
2	2	2408	158	0.39
3	2	3365	158	0.22
4	2	4322	158	0.12
1	3	1698	136	0.36
2	3	2655	136	0.26
3	3	3612	136	0.17

Table 2: Fitting parameters of the multi-phonon fitting model for one till four phonons of 957 cm^{-1} with zero till four 247 cm^{-1} phonons.

5.1.4 Fluorescence measurements

Since the absorption spectrum of the Si Ncs is known, the Si Ncs can be excited in order to measure the fluorescence. The fluorescence is measured with two different setups as described in sections 4.1.2 and 4.1.3. Firstly, the fluorescence was measured, using a Fluorlog spectrometer, between 30000 and 38500 cm^{-1} (260 nm to 330 nm with several nm resolution). This result is shown in Fig.(12).

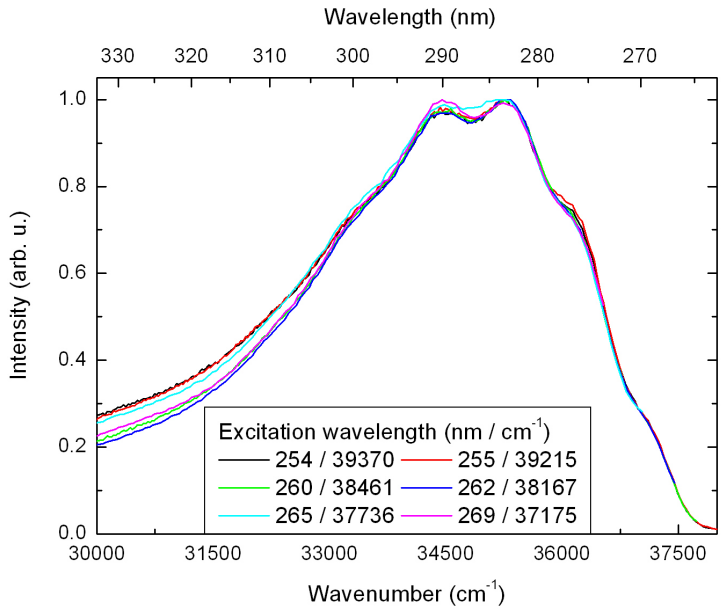

Figure 12: Fluorescence of Si Ncs at different excitation wavelengths. It can be observed that the fluorescence is virtually excitation wavelength independent.

From this figure it can be observed that the fluorescence spectrum contains some structure, though less detailed compared to the absorption spectrum. The fluorescence spectrum could be inhomogeneously broadened because of several factors: the interaction with the solvent is higher in the excited state, Si Ncs do not relax to the lowest vibrational level of the excited state before emitting or the size distribution of the Ncs is more influential for the fluorescence spectrum. Since most of the fluorescence takes place from the

lowest vibrational level of the excited state to the vibrational levels of the ground state, the fluorescence spectrum probes the structure of the ground state.

To investigate whether or not the wavelengths at which the fluorescence occurs change as function of the excitation wavelength, the fluorescence is recorded by exciting at the wavelengths of several absorption peaks (254, 255, 260, 262, 265 and 269 nm). As can be observed in Fig.(12), the fluorescence is virtually excitation wavelength independent. This result can be have several interpretations. Firstly, the Si Ncs could be nearly perfectly monodispersed. Secondly, only one size Si Ncs could be fluorescent. Thirdly, the emission wavelength could be weakly size dependent. And finally, the emission could originate on the surface of the Si Ncs (e.g. in Si - C bonds). To improve the resolution of the fluorescence measurements, the fluorescence is recorded using the OMA as described in 4.1.3. The result of this measurement is depicted in Fig.(13).

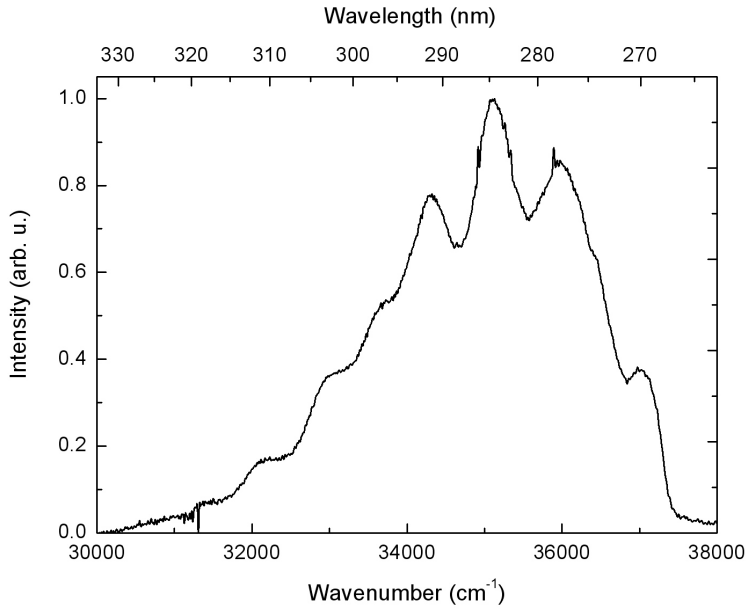

Figure 13: Fluorescence of the Si Ncs, excited at 250 nm, detected by OMA.

The resolution of this measurement is approximately 0.6 nm (58 cm^{-1} at

260 nm). Also in this figure the fluorescence is less structured, compared to the absorption spectrum, although more structured compared to Fig.(12). The peaks are still much broader than in the absorption spectrum, although the width of the fluorescence peaks is not determined by the resolution of the system.

5.1.5 Frank-Condon fluorescence fitting

From the fitting of the fluorescence two uncoupled phonon frequencies are obtained, 660 cm^{-1} and 900 cm^{-1}. The result of this fit is shown in Fig.(14).

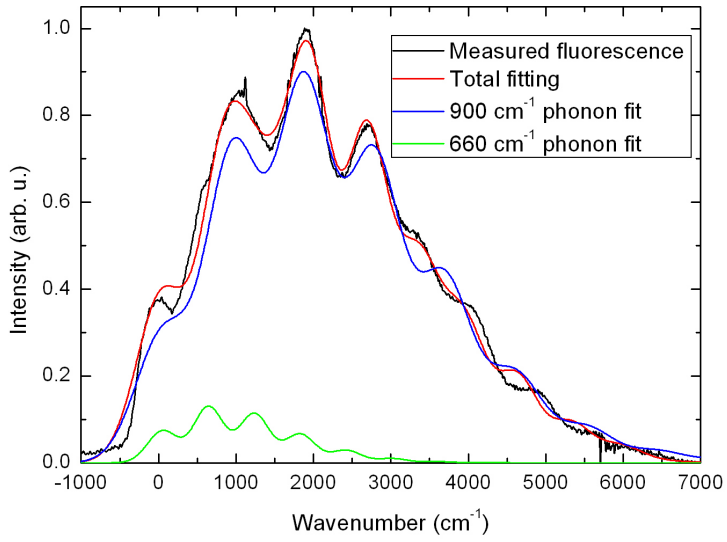

Figure 14: This figure shows the fluorescence (black curve) and the fit of the fluorescence (red curve) by means of two uncoupled phonons of 660 cm^{-1} (green curve) and 900 cm^{-1} (blue curve).

The peak widths of the two progressions are 465 and 357 cm^{-1}. The phonon frequency of 900 cm^{-1} could correspond to the same phonon frequency of the absorption of 957 cm^{-1}. The 660 cm^{-1} can correspond to the 659 cm^{-1} measured with Raman scattering spectroscopy. It can be observed that the fit corresponds to the measured fluorescence relatively well. The discrepancy

of the fit can be due to the fact that the Frank-Condon model is a simple model which convolves the Frank-Condon factors with gaussian lineshapes. The assumption that the shape of the peaks is gaussian can be incorrect and a combination of gaussian and lorenzian functions should be used.

5.1.6 Mirror image of absorption and fluorescence

As described in the previous sections, the structure of the absorption spectrum indicates the vibrational structure of the excited state (due to the transitions from the ground state to the vibrational level of the excited state) and the fluorescence spectrum gives an indication of vibrational ground state structure (due to transitions from the lowest vibrational level of the excited state to the vibrational levels of the ground state). Assuming that the potential landscape of the Si Ncs is not changing much after electronic excitation, the structure of the absorption spectrum should be similar to the mirror image of the fluorescence spectrum. Fig.(15) shows the absorption (red curve) and fluorescence (black curve) spectra of the Si Ncs.

To compare to what extend the fluorescence spectrum coincides with the absorptions spectrum, the absorption spectrum is mirrored over the first clearly visible peak at approximately 37010 cm^{-1}, the zero-phonon line, and placed onto each other. This result is shown in Fig.(16). The peak positions of the peaks which are most likely the zero-phonon lines of the absorption and fluorescence spectrum respectively, are determined at 37010 and 37259 cm^{-1}. This difference in peak position is called the Stokes shift and is determined to be 240 cm^{-1}.

This figure shows that the first two absorption peaks coincide with the first two fluorescence peaks. Later on, three or more absorption peaks overlap with one fluorescence peak. It can be concluded that the overall shape the absorption and fluorescence spectrum are nearly mirror images. Thus, the potential structure of the ground state and the excited state are similarly shaped.

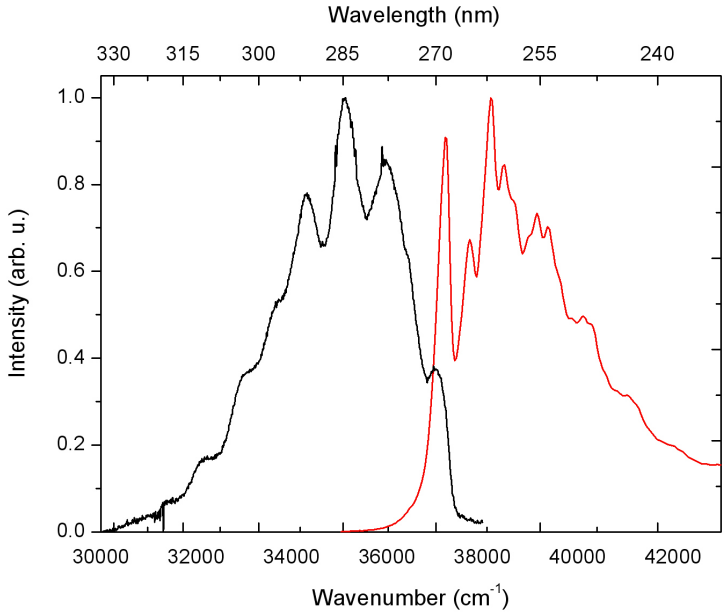

Figure 15: This figure represents both the fluorescence spectrum (black curve) and the absorption spectrum (red curve) of the Si Ncs. From this figure the Stokes shift is determined to be approximately 240 cm^{-1}.

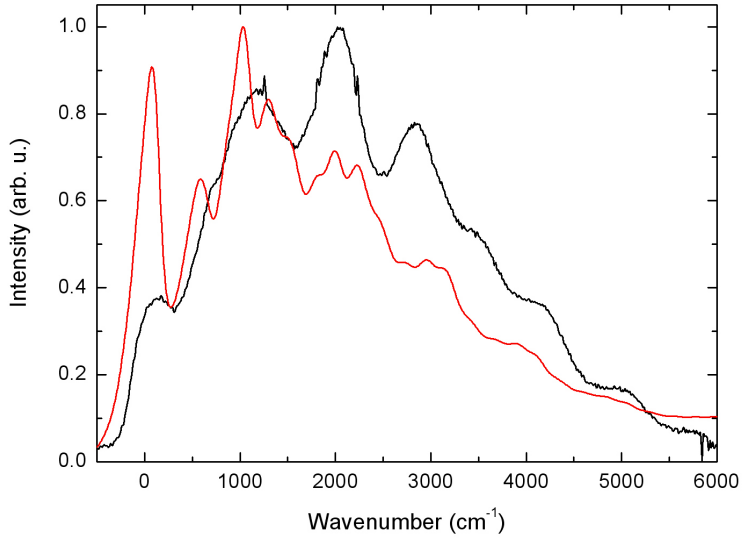

Figure 16: The absorption spectrum (red curve) is mirrored over the zero-phonon line and positioned on top of the fluorescence spectrum (black curve). It can be observed that the position of the main peaks of the absorption and the fluorescence spectra are in the same vicinity.

5.1.7 Raman scattering spectroscopy

The distances between the peaks of the absorption and the fluorescence spectra can possibly have the following physical interpretation. These distances can be the vibrational modes of the Si Ncs. To determine these modes, Raman and infra-red (IR) spectroscopy is performed, in order to find possible observed frequency modes. This section will discuss the Raman spectroscopy. As described in section 4.1.4 Raman spectroscopy measures the energies of Raman active vibrational of the ground state.

To determine the response of the Si Ncs the spectra of the solvent (hexane) and the Si Ncs in solvent are recorded. This to correct the measurements for the influence of the solvent. Raman spectroscopy performed on the Si Ncs shows with respect to hexane two additional frequency modes, namely at 259 cm^{-1} (38.6 μm) and 652 cm^{-1} (15.3 μm), as shown in Fig.(17). The 259 cm^{-1} peak originate from the vibrational modes of Si Ncs. The 652 cm^{-1} is determined to originate from $C_{10}H_{21}$, since Raman spectroscopy on Si Ncs with C_6H_{13} does not show a peak at this position.
These two modes can be assigned to the functionalization of the shell and the core of the Si Ncs. To determine which frequency mode is due to the functionalization, Raman spectroscopy on Si Ncs with other functionalization has to be performed. In addition, the 259 cm^{-1} corresponds relatively well to the peak distances of 247 cm^{-1} of the absorption spectrum. This can suggest that this is the same the vibrational mode. The difference occurs from the fact that absorption spectroscopy probes the excited state, while Raman spectroscopy was performed in the ground state.

5.1.8 Infrared absorption spectroscopy

To study the vibrational ground state levels more extensively, infrared ground state measurements on the Si Ncs are performed. This is achieved by performing FT-IR spectroscopy. For the Raman measurements the standard cell (FUV quartz cuvette) was used. Since quartz is not transparent in infrared, other methods must be used in order to perform the IR measure-

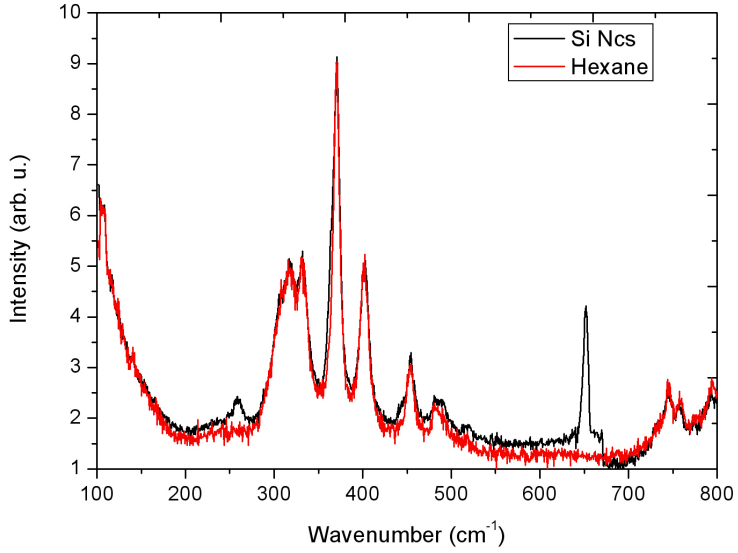

Figure 17: Raman spectrum measured for both the solvent (hexane) and the Si Ncs. In the Si Ncs spectrum, at 259 cm^{-1} and 652 cm^{-1}, peaks are clearly visible. The 259 cm^{-1} peak originate from the vibrational modes of the Si Ncs and the 652 cm^{-1} is from the $C_{10}H_{21}$ functionalization.

ments. Therefore, Si Ncs are drop casted on a Potassium-Bromine (KBr) wafer and the solvent (hexane) is evaporated during this procedure. The spectrum recorded by this measurement is shown in Fig.(18).

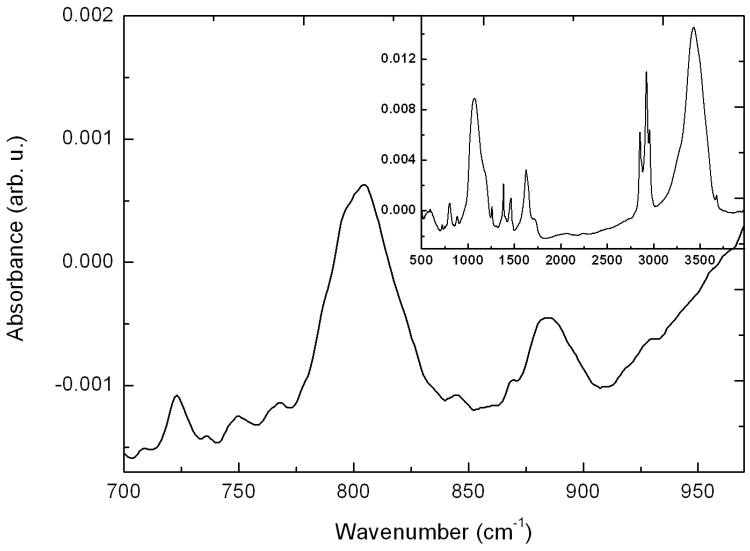

Figure 18: Infrared spectrum measured with a Fourier-transform infrared spectrometer on a KBr wafer (inset). The peak at 805 cm^{-1} is absorption of the Si Ncs and the other peaks correspond to the absorption of the KBr substrate, n-decyl functionalization, water and other contaminants.

Many peaks can be observed in this figure. The peaks around 805 cm^{-1} (12.5 μm) are the only peaks which can only be assigned to Si Ncs. The other peaks are coming from the n-decyl functionalization, KBr wafers, water and other contaminants. In the spectrum the 957 cm^{-1} mode of the absorption spectrum is absent.

5.2 Time-resolved spectroscopy

The following sections will discuss the time-resolved fluorescence and the results of the pump-probe measurements, in order to obtain the spectral dynamics of the Si Ncs. The description of the corresponding experimental setups can be found in section 4.2.

5.2.1 Time-resolved fluorescence

The setup as described in section 4.2.1, is used to measure time-resolved fluorescence. The goal of this measurement is to determine the excitation decay time constant of the Si Ncs. The decay time constants for different sizes Si Ncs should be different, so if the Si Ncs are not single-sized, poly-exponential decay dynamics is expected. Time-resolved measurements are also performed to determine whether or not the fluorescence decay is excitation wavelength independent within the absorption range. The results of the time-resolved fluorescence measurements are shown in Fig.(19).
The measured fluorescence decay dynamics is monoexponential. The decay time constant is 5.7 $\pm$ 0.2 ns, for excitation frequencies of 254 and 269 nm. This single exponential decay dynamics can have several explanations as discussed in section 5.1.4 on the CW fluorescence: firstly, a nearly perfectly monodispersed Si Ncs in size, secondly, only one size Si Ncs could be fluorescent, thirdly, the emission wavelength could be weakly size dependent, and finally, the emission could originate on the surface of the Si Ncs (e.g. in Si - C bonds).

The fluorescence decay is also excitation wavelength-independent, since excitation by 254 nm and 269 nm pump beam yields the same fluorescence decay. In addition to this, the decay-time constant shows no excitation power dependence, up to several photons per excitation pulse per Nc. Unfortunately, higher energies per pulse could not be reached in mid-UV.

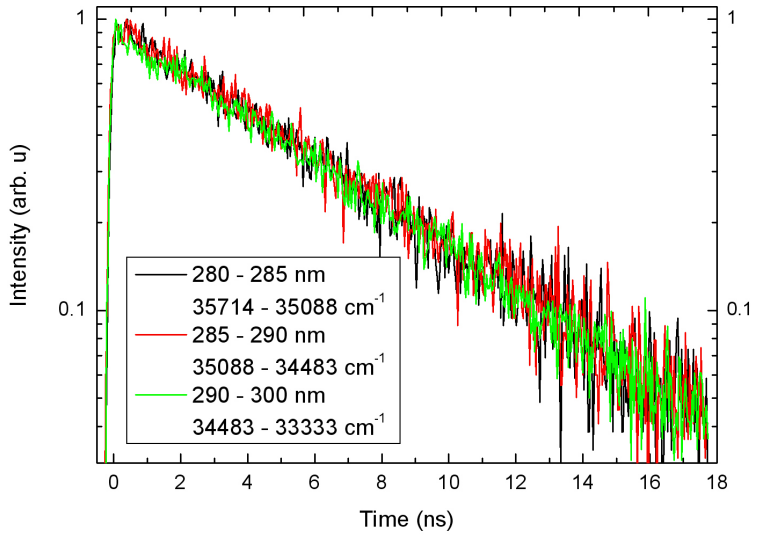

Figure 19: This figure shows fluorescence dynamics of the Si Ncs for different spectrum slices of 280 to 285 nm (black curve), 285 to 290 nm (red curve) and 290 to 300 nm (green curve). The excitation wavelength is 269 nm. The fluorescence decay of the Si Ncs is monoexponential with a time constant of 5.7 $\pm$ 0.2 ns.

5.2.2 Time-resolved transient absorption spectroscopy

To obtain information about the fast dynamics of the Si Ncs, time-resolved transient absorption spectroscopy is performed. The measurements are recorded from 2 ps before the pump-pulse excites the Si Ncs till 12 ps after excitation. See Fig.(20) for a typical scan of the time-resolved transient absorption signal. This signal seems noisy, but since this signal contains a lot of data points the average of the signal can be determined with a relative small error in ΔOD of $1{\cdot}10^{-4}$.

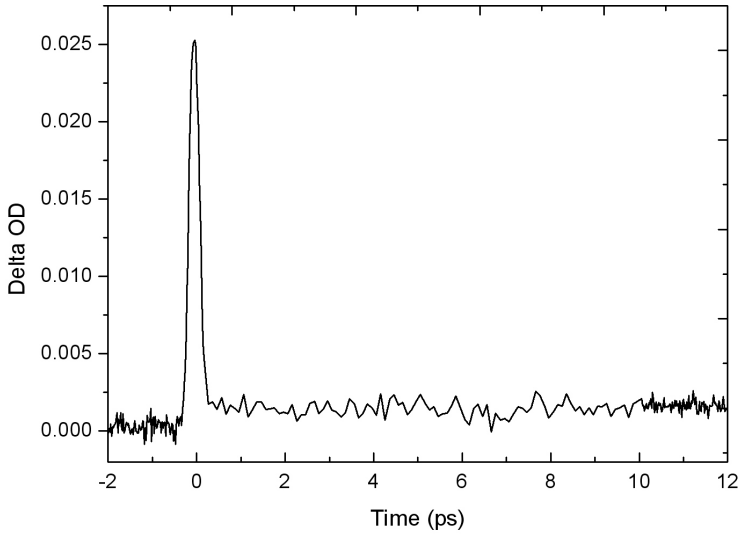

Figure 20: A typical single scan time-resolved transient absorption signal, with a pump wavelength of 250 nm and a probe wavelength of 290 nm.

The ΔOD is measured in Fig.(20). A positive signal is shown in this figure, which means that stimulated absorption occurs in the sample. As described in chapter 3, some electrons are excited to the first excited state, but in this case, apparently, the absorption probability to the higher excited states is larger than from the ground state. This results in a positive pump-probe signal. The pump-probe signal shows that within the time resolution of 200 fs, no dynamics, except of coherent artifact within the time overlap of pump

and probe pulses, was observed. Therefore, the signal is flat in the recorded range. The Si Ncs are pumped at 250 nm with an 10 μW beam. The ΔOD is determined from 10 ps to 12 ps. Fig.(21) shows the ΔOD obtained by the pump-probe measurements at different probe energies.

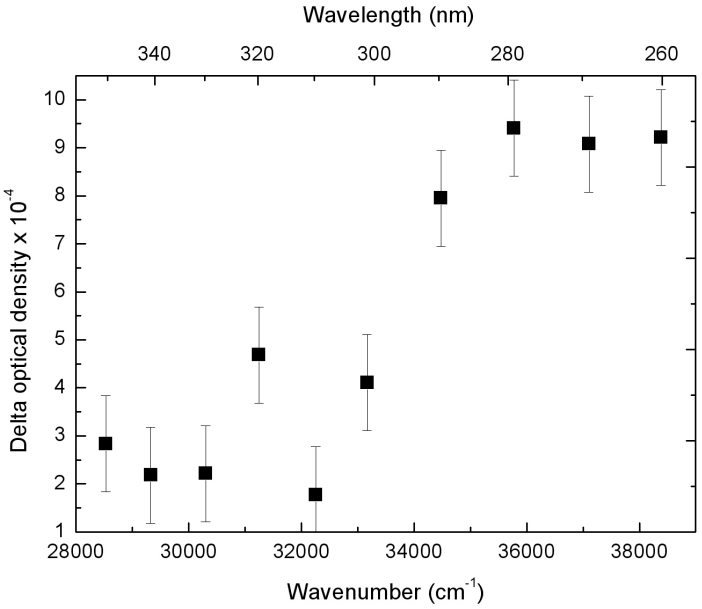

Figure 21: Transient absorption integrated between 10 ps to 12 ps after excitation. The Si Ncs are pumped at 250 nm with an 10 μW beam.

Time-resolved transient absorption spectroscopy shows strong stimulated absorption in the absorption range (34000 and 38000 cm^{-1}). Outside this range, stimulated absorption decreases steeply. Below 12500 cm^{-1} no significant response is observed. No bleaching was observed in the whole spectral range from 250 to 800 nm.

6 Discussion and Conclusions

Quantum dots produced for scientific and commercial applications [1] are dispersed in size by at least 5 to 10 % [2]. To obtain single sized quantum dots, filtering is applied. This is an inefficient method to produce large quantities. It would be a breakthrough to control a method to produce large quantities of single sized quantum dots [26]. The described measurements strongly support to the conclusion that the Si Ncs are monodispersed.

The support for this conclusion can be found in several measurements. Firstly, the line-width () of the absorption peaks is less than 200 cm^{-1} at an energy (E) in the region of 40000 cm^{-1}. So the ratio $\frac{\Delta E}{E}$ is approximately 0.01 %. The confinement energy scales with $E \propto \frac{1}{R^2}$, with R as the diameter of the Si Ncs. Therefore, the distribution in size can be indicated using the expression $\frac{\Delta E}{E} = \frac{2 \cdot \Delta R}{R}$. Neglecting all the other factors, such as temperature and solvent effects, which contribute to the broadening of the spectrum, this indicates the size distribution to be better than 0.01 %, which represents less than one atom difference per Si Ncs.

The suggestion of a very well determined size of Si Ncs does not exclude the concept of having a few well determined sizes of Si Ncs, all contributing to different spectral peaks of the absorption and fluorescence spectra. This concept is rebutted by the following three reasons. Firstly, the CW fluorescence measurements show that the fluorescence spectrum is excitation wavelength independent. Secondly, the time-resolved fluorescence shows that the fluorescence decay is mono-exponential at all fluorescence wavelengths. Thirdly, the fluorescence dynamics is excitation wavelength independent. This can be explained by several reasons. Firstly, only the same size Si Ncs are fluorescent. Secondly, different types of Si Ncs are fluorescent with accidentally the same wavelengths, what is unlikely. Thirdly, strong energy coupling between separate Si Ncs results in size independence of the fluorescence. This is unlikely, since the decay time constant is 5.7 $\pm$ 0.2 ns, but the timescale

of energy hopping between the Ncs, estimated using Foerster dipole-dipole energy transfer model, is in the order of several milliseconds.

IR measurements show at 805 cm^{-1} an active Si Ncs mode. Due to disturbance of the electronic excited state by the excitation, these frequency modes are considered to originate from the same vibrational mode. The absorption spectrum contains a structure periodicity of 957 cm^{-1}, starting from the zero-phonon line. The multi-phonon fitting model shows that the absorption spectra is dressed with an additional sharp structure of 247 cm^{-1} between the peak positions. Raman spectroscopy shows a vibrational mode at 259 cm^{-1}. Also these modes are considered to originate from the same vibrational mode. The fluorescence fittings show two uncoupled phonon frequencies of 660 and 900 cm^{-1}. The 660 cm^{-1} of the fluorescence spectrum corresponds possibly to the 659 cm^{-1} mode measured with Raman scattering spectroscopy.

From the absorption and fluorescence measurements it is observed that the zero-phonon lines of the spectra are shifted merely by approximately 240 cm^{-1}. This implies, together with the small Stokes shift, that the electronic ground state and the electronic excited state are nearly at the same position.

The transient absorption at 260 till 300 nm is large. Outside this range the transient absorption is small. The signal of the transient absorption is positive in all the measured range. Thus, the excited states absorb more photons compared to the ground state. This implies that the energy spacing of the excited states is less with respect to the energy spacing of the ground state and the first excited state.

It can be concluded that the Brownian oscillator model is correct in the physical sense. The absorption fitting obtained from this model is considered to be not completely correct, since it is making use of six or more independent phonons. The large amount of phonons needed to fit the spectrum well is in contradiction to the measured number of frequency modes observed in

Raman and IR spectra. This discrepancy originates possibly from the low temperature assumption of the model or that the phonons frequencies are not coupled in this fitting model.

The multi-phonon fitting model fits the measured absorption spectrum very well, but it can not be concluded that the multi-phonon fitting is physically better than the Brownian oscillator. The reason for this is that the multi-phonon fitting model does not predict the amplitudes of the peaks correctly. The model fits the absorption spectrum with two phonon frequency modes of 957 cm^{-1} and 247 cm^{-1}, the fluorescence can be fitted with 660 cm^{-1} and 900 cm^{-1}. The expected cross-section of transitions which involve a combination of up to five phonons for each type is relatively low. The two phonon frequencies from this fitting are in perfect correspondence to the measured phonon frequencies.

7 Acknowledgments

Looking back on my research project, I realize that I could never have completed this research without the valuable help of many people. I appreciate the contribution to my research of all of them and I want to express my gratitude to the following persons in particular.

Fist of all my coaches Ramunas Augulis and Pedro Rizo. I will start with Ramunas. He has been of great help to me on both the technical and the theoretical part of my research project. Together we performed many experiments and we spend a lot of time in the laboratories. He taught me how to work with lasers and all kind of other optical equipment. I enjoyed working together with him a lot, he was a great teacher for me. Pedro has been of great help to me, more at the theoretical side of this research. By strengthening with good thoughts and ideas. It was a great pleasure to work with Ramunas and Pedro and to have them as coaches. Paul van Loosdrecht was always interested to take a look at the results. Many fruitful discussions have past and gave deeper insight in the results. I am thankful for the opportunity to perform my master research at his group.

The samples were synthesized by Milena Rosso-Vasic under supervision of Han Zuilhof from the University of Wageningen. The collaboration with them was very pleasant and useful. I am thankful for the provided samples and to my understanding the Silicon nanocrystals are also from the physical point of view beautiful. Daniele Fausti employed his Raman setup to provide the Raman results. Thanks for helping me with this.

The technical staff helped me a lot. Ben Hesp was of great help with many experiments. Especially for the possibility to use his setup and the usage of the streak camera I am thankful of. Foppe de Haan wrote all kind of nice programs and he helped me fitting the experimental results, even on Sunday, together with Maxim Pchenitchnikov. Arjen Kamp struggled with the Bomem IR-spectrometer and with polyethylene cells for my aid, thanks

a lot for this great effort. The research group in total was really nice. I enjoyed the coffee breaks in my 'office', the lunch breaks and the activities after working hours. I am sure that I will long back to the past times in the cellar of building 17 ones in the future.

Indirectly I was supported by my family. They were always interested and supported me along the long route I took in studies. Thanks a lot for stimulating and guiding me. Especially I would like to express my appreciation for the support Lian gave during my study. I look forward to our new future together.

References

[1] Evident Technologies, New York

[2] W.W. Yu et al., Chem. Mater. **15**, 2854-2860, 2003.

[3] M. Rosso-Vasic et al., Alkyl-functionalized oxide-free silicon nanoparticles: synthesis and optical properties, (submitted to SMALL, 2007).

[4] L.T. Canham, Appl. Phys. Lett., **57**, 1046, 1990.

[5] R.D. Tilly et al., Chem. Commun., 1833 - 1835, 2005.

[6] X. Li et al., Langmuir, **19**, 8490, 2003.

[7] K.A. Littau et al., J. Phys. Chem., **97**, 1224, 1993.

[8] H. Takagi et al., Appl. Phys. Lett., **56**, 2379, 1990.

[9] J. Wang et al., Bioconjugate Chem., **15**, 409, 2004.

[10] J.D. Holmes et al., J. Am. Chem. Soc., **123**, 3743, 2001.

[11] Wageningen University, Laboratory of Organic Chemistry, Research group of H. Zuilhof, http://www.orc.wur.nl/UK/.

[12] R.L. Liboff, Introductory Quantum Mechanics, Addison Wesley, 2002.

[13] Al.L. Efros and A.L. Efros, Sov. Phys. Semicond., **16**, 772, 1982.

[14] M.C. Beard et al., Nano Letters, **7**, 2506, 2007.

[15] W.A. Harrison, Electronic Structure and the Properties of Solids, Dover New York, 1989.

[16] A. Puzder et al., J. Am. Chem. Soc. **125**, 2786, 2003.

[17] C.W. Fischer, Am. J. of Phys, **50**, 1103, 1982.

[18] Ioffe Institute, www.ioffe.ru/sva/nsm/semicond/si/figs/121.gif.

[19] C. Delerue et al., Physical Review B, **48**, 15, 1993.

[20] M.L. Mandich et al., Z. Phys. D., **26**, 147, 1993.

[21] R. Hull, Properties of Crystalline Silicon, INSPEC, New York, 1987.

[22] P. Atkins, Physical Chemistry, Oxford University Press, 2002.

[23] S. Mukamel, Principles of Nonlinear Optical Spectroscopy, Oxford University Press, 1995.

[24] Fausti et al., Phys. Rev. B., **75**, 245114, 2007.

[25] H. Kuzmany, Solid State Spectroscopy; An introduction, Springer-Verlag, 1998.

[26] J.R. Mialichil et al., Journal of Materials Science, **43** 568, 2008.